μMote: Enabling Passive Chirp De-spreading and μW-level Long-Range Downlink for Backscatter Devices

Yihang Song and Li Lu, *University of Electronic Science and Technology of China;* Jiliang Wang, *Tsinghua University;* Chong Zhang, Hui Zheng, and Shen Yang, *University of Electronic Science and Technology of China;* Jinsong Han, *Zhejiang University;* Jian Li, *University of Electronic Science and Technology of China*

https://www.usenix.org/conference/nsdi23/presentation/song-yihang

This paper is included in the
Proceedings of the 20th USENIX Symposium on
Networked Systems Design and Implementation.

April 17–19, 2023 • Boston, MA, USA

978-1-939133-33-5

Open access to the Proceedings of the
20th USENIX Symposium on Networked
Systems Design and Implementation
is sponsored by

μMote: Enabling Passive Chirp De-spreading and μW-level Long-Range Downlink for backscatter Devices

Yihang Song[1], Li Lu[1], Jiliang Wang[2], Chong Zhang[1], Hui Zheng[1], Shen Yang[1], Jinsong Han[3], and Jian Li[1]

[1]University of Electronic Science and Technology of China
[2]Tsinghua University
[3]Zhejiang University

Abstract

The downlink range of backscatter devices is commonly considered to be very limited, compared to tremendous long-range and low-power backscatter uplink designs that leverage the chirp spread spectrum (CSS) principle. Recently, some efforts are devoted to enhancing the downlink, but they are unable to achieve long-range receiving and low power consumption simultaneously. In this paper, we propose $\mu Mote$, a μW-level long-range receiver for backscatter devices. $\mu Mote$ achieves the first passive chirp de-spreading scheme for negative SINR in long-range receiving scenarios. Further, without consuming external energy, $\mu Mote$ magnifies the demodulated signal by accumulating temporal energy of the signal itself in a resonator container, and meanwhile it preserves signal information during this signal accumulation. $\mu Mote$ then leverages a μW-level sampling-less decoding scheme to discriminate symbols, avoiding the high-power ADC-sampling. We prototype $\mu Mote$ with COTS components, and conduct extensive experiments. The result shows that $\mu Mote$ spends an overall power consumption of $62.07\mu W$ to achieve a $400m$ receiving range at a $2kbps$ data rate with 1% BER, under $-2dB$ SINR.

1 Introduction

Backscatter communication has significant advantages over active radio in terms of power consumption. The recognized drawback of conventional backscatter devices [10, 46] is their insufficient communication range of only a few meters. In the last decade, a number of long-range backscatter techniques [23, 35, 37, 51, 54, 55] are proposed that can significantly increase the uplink backscatter range to hundreds of meters or even more than $1km$. Their main idea is to reflect the Chirp Spread Spectrum (CSS) signal. When this chirp signal is de-spread by the gateway receiver, it will incur a processing gain for the receiver, and therefore more interference immunity and longer communication range.

Nevertheless, the downlink range of this type of long-range backscatter devices [18, 37] is limited to less than 20 meters [17]. As they still use the conventional envelope detector as a receiver [15, 30], rather than de-spreading the chirp signal. In the last two years, two efforts are devoted to extending the downlink range. Saiyan [17] leverages an RF band-pass filter (with $6dB$ signal strength loss) to assign an envelope to the chirp signal, and subsequently uses an envelope detector to detect the assigned envelope. This demodulation method does not de-spread the chirp signal, so it cannot obtain processing gain and extend the downlink range. Instead, to extend the range, Saiyan uses an LNA (Low Noise Amplifier) and an OP AMP (Operational Amplifier) to amplify the signal [16, 21, 40] and gains a receiving range of $180m$. However, these two amplifiers consume about $88mA$, which is similar to the current consumption of active radio, and 176 times that of the typical backscatter device [46]. Passive-DSSS [31] employs two envelope detection channels to transmit DSSS (Direct Sequence Spread Spectrum) spreading codes, enabling anti-interference receiving. However, it strictly requires a positive SINR. Besides, due to the performance limitation of the envelope detector, its downlink range is limited to about 50 meters, far less than the uplink range of existing long-range backscatter devices. Therefore, to the best of our knowledge, none of existing envelope detector-based receivers can achieve long-range receiving with low power consumption.

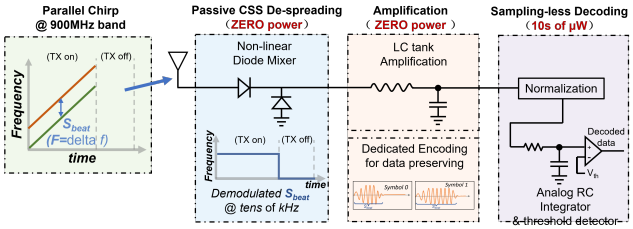

Figure 1: **The high-level block diagram and basic principle of $\mu Mote$.**

In an IoT network consisting of backscatter devices and a gateway, insufficient downlink range will be the bottleneck of network coverage. When a backscatter device is placed far away from the gateway, the incapability of downlink communication can lead to the failure of essential network func-

tions, including ACK and re-transmission [13], multi-access control [13], network association [27], over-the-air firmware switching or updating [59, 60], and device authentication [41].

Conventional methods to improve the downlink range can be classified into two categories. The one is to employ spread spectrum communication to suppress interference, so as to demodulate the signal at low SINR (signal-to-interference-plus-noise ratio) or even negative SINR. The other one is to use amplifiers (i.e., LNAs) [58] to enhance the receiver sensitivity and combat signal strength loss during propagation. De-spreading the spread spectrum signal, e.g., the CSS signal, requires a local-generated carrier and correlated de-spreading signals, which will incur very high power consumption (e.g., more than $7mW$ [6]). As for LNAs, by their nature (see Sec. 2.1), they commonly consume $10mW$ to more than $100mW$ [14, 47]. In summary, these two solutions are very power-consuming, and therefore cannot realize on backscatter devices whose overall power consumption is commonly less than $1mW$ [46].

In this paper, we present *µMote*, a μW-level re*Mote* receiver with hundreds of meters of receiving range, which can effectively work even under negative SINR. The high-level idea incorporates three key designs, as shown in Fig. 1: a novel Passive Chirp Spread Spectrum (Passive-CSS) de-spreading design to combat interference, a magnification scheme to magnify the demodulated signal with zero external power consumption to combat signal strength loss, and an efficient decoding design with only tens of μW.

More specifically, *µMote* addresses the following key challenges.

(1) How to address interference or even negative SINR with extremely low power? We try to leverage Chirp Spread Spectrum (CSS) technique to resist interference, which has been widely used in backscatter transmitters. Existing chirp de-spreading techniques, however, consume very high power consumption, as we describe above. To this end, we present the first Passive Chirp Spread Spectrum (Passive-CSS) technique, which removes the conventional power-consuming chirp demodulation and de-spreading processes. The basic idea is a parallel chirp modulation scheme for the gateway and then a passive chirp de-spreading circuit with zero power. Thus, we can passively decode the chirp signal while retaining the long-range and interference-resilient features.

(2) How to increase the signal amplitude without external power, and meanwhile preserve signal information? Traditional amplification solutions, such as LNAs, commonly consume more than ten mW of power. To solve this problem, we leverage an *LC* resonator (also called *LC* tank) as a container to accumulate the energy of demodulated signal so as to magnify the signal amplitude. However, when the signal energy is stored in such an *LC* tank, the corresponding signal information that is supposed to be in chronological order can be overlapped and distorted. To preserve the information, we expect a new encoding method that can embed information into the accumulated signal. Inspired by PIE (Pulse Interval Encoding), we propose a software/hardware co-designed encoding scheme that leverages the duration of the magnified signal to represent symbols.

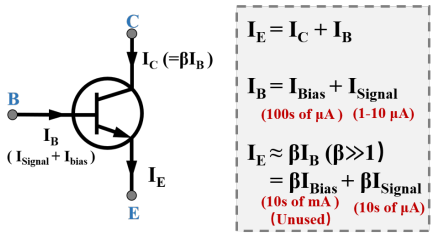

Figure 2: **Amplification principle and current consumption of an LNA.**

(3) How to efficiently decode symbols conveyed by the magnified signal? Existing receivers usually employ ADC for high-speed sampling and decoding. This accounts for the vast majority of the power consumption of backscatter devices. For example, a widely used low-power integrated ADC IC [49] typically consumes hundreds of μW power. In this paper, we present an analog *RC* integrator to decode without the need for ADC. This significantly reduces the power consumption to several μW. Specifically, we introduce a low-power energy integrator to identify the symbols based on the level of symbol energy. Moreover, the above circuit is designed to be programmable to achieve ADC-free symbol synchronization before decoding. Besides, we present a normalization scheme to address the "dynamic symbol energy" problem caused by the diversity of signal strength.

Summary of the contributions and results:

- We propose the design of *µMote*, a novel μW-level low-power receiver with hundreds of meters of receiving range which can effectively resist interference and work even under negative SINR.

- We address the fundamental challenges for realizing the receiver. We realize a passive-CSS communication technique on passive circuits, enabling zero-power chirp de-spreading and demodulating. We present the zero power magnification scheme by accumulating the energy of the demodulated signal itself. And we propose the design of a sampling-less analog energy integrator for μW symbol decoding.

- We prototype *µMote* with COTS components and conduct extensive experiments. The results demonstrate that *µMote* reaches a communication range of more than $400m$ at a 1% Bit Error Rate (BER) with an average working power of $61.07\mu W$. Compared to the literature of existing works [17, 31], *µMote* improves the downlink range by $2.5\times$ to $8.65\times$, with a power consumption reduction of at least 63.2%. Under the case of narrowband

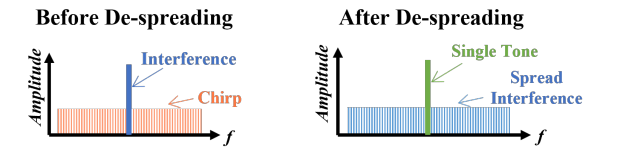

(a) Spectrum of chirp and interference before and after de-spreading

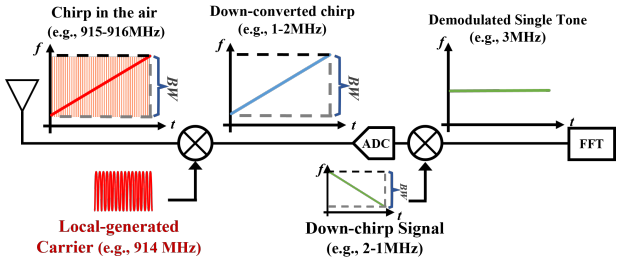

(b) Procedures of conventional chirp de-spreading.

Figure 3: **Principle of conventional chirp de-spreading, in which the power consumption of carrier generation is not affordable for backscatter devices.**

interference, *μMote* can work at $-2dB$ SINR or above. To the best of our knowledge, this is the first receiver that can work under negative SINR with μW-level power.

2 Background and Motivation

Before presenting our design, it is worth investigating why existing receivers cannot achieve long-range receiving with low power consumption. We classify existing approaches to long-range receiving into two categories: amplifying the signal and spreading spectrum technique.

2.1 Amplifying the Signal

Receivers usually use LNAs to amplify the received signal strength, as LNAs' low noise figure can minimize the noise caused by the amplification process. An LNA usually consists of multiple triodes and peripheral analog circuits. Its function of signal amplification is performed by the triodes. Fig. 2 depicts the principle of a triode. By leveraging the external current injected to its collector (I_C), it can amplify small base current (I_B) by β times, and the amplified current is output as emitter current I_E, i.e.,

$$I_E = I_C + I_B = \beta I_B + I_B \approx \beta I_B (\beta \gg 1)$$

where the β inherently depends on the transistor and can be typically large up to 100.

However, the practical power efficiency of such triodes is very low. As shown in Fig. 2, the I_B contains not only the signal current (I_{Signal}), but also a bias current (I_{Bias}) that is significantly larger than I_{Signal}. The I_{Bias} contains no signal information but can ensure that the triode works within the linear active region (amplifying region). After amplification, the amplified I_{Bias} will be removed. In the widely used commercial LNA ICs [7, 8], the I_{Bias} is commonly hundreds of μA or even more than $1mA$. Hence, amplifying the I_{Bias} makes commercial LNA ICs consume several mA to even hundreds of mA of external current. As a comparison, the total power consumption of a typical backscatter device is $470\mu A$ [46].

2.2 Spread Spectrum Technique

Spread spectrum techniques, such as Chirp Spread Spectrum, has been widely used in LPWAN (Low Power Wide-Area Network) and backscatter transmitters due to their interference immunity and long communication range. In brief, the basic idea of CSS is "don't put all the eggs into one basket". Specifically, by transmitting or reflecting the wide-band chirp signal, the information (e.g., a symbol) is distributed to the chirp's band (the red shaded area in Fig. 3(a) and Fig. 3(b)). Hence, the narrow-band interference is unable to cover the entire band, even if it has a stronger signal strength, as shown in Fig. 3(a).

The receiver needs to de-spread the chirp to gather the distributed information. As shown in Fig. 3(b), the chirp is down-converted to a relatively low frequency (e.g., 1–$2MHz$) and then multiplied by a down-chirp signal, incurring a single tone signal which sums the frequency of the down-chirp and the down-converted chirp. Meanwhile, the narrow-band interference is also multiplied by the down-chirp signal, but then its energy is spread into the entire chirp's band. This means the single-tone signal gains high SINR and can be easily recognized by FFT (Fast Fourier Transform) operation (as shown in Fig. 3(a)). With the FFT results, the receiver knows whether a chirp is transmitted or not, even if the chirp has lower strength than that of the interference.

Nevertheless, the conventional chirp de-spreading process is power-consuming, as it requires the receiver to generate the high-frequency carrier for down-conversion and perform FFT operation. Generating the carrier needs power-consuming components, such as the VCO (Variable Crystal Oscillator) and the PLL (Phase Locked Loop), and performing FFT requires high-speed computing. These operations inevitably incur high power consumption that is undesirable for backscatter devices [29, 34]. Hence, chirp de-spreading has never been implemented on backscatter devices.

2.3 Motivation

After revisiting existing solutions and their power consumption, we aim to design a receiver with interference resistance, long-range receiving (high receiving sensitivity), and low-power consumption. We are motivated to take the following strategies to solve those problems, respectively.

Interference resilience: When the receiver is far away from the gateway, the received signal becomes susceptible

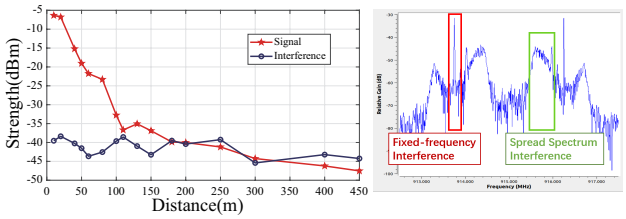

(a) (b)

Figure 4: **(a) Site survey for the strengths of ambient interference and downlink signal in the campus environment, and (b)Then measured spectrum of interference signals.**

to interference. This significantly decreases the receiving performance in practice, especially for non-noise-resistant envelope detectors. Hence, we are motivated to present a passive chirp de-spreading design to combat interference.

Low-power Magnification: Amplification can combat signal strength loss and improve receiving range. However, using LNAs can cause enormous power consumption. Thus, we present the LNA-free magnification scheme with zero power consumption, which helps to extend the receiving range.

Low-power decoding: Conventional symbol decoding solution is high-speed ADC sampling. However, it typically consumes hundreds of microwatts, accounting for the major part of the power consumption of a backscatter device [46]. Hence, we expect a power-efficient decoding mechanism without high-speed ADC sampling.

3 Passive Chirp De-spreading

The envelope detector is widely used in low-power receivers as it requires no high-power-consuming components and computing tasks. However, the envelope detector is subject to interference. When the interference is stronger than the downlink signal, it will misidentify the envelope of interference as the envelope of the downlink signal, thereby incurring communication failure. To better understand this, we conduct a preliminary site survey in a campus environment. As illustrated in Fig. 4(a), at the distance of 250m, 350m and above, the interference strength is stronger than that of the signal. In those environments, the envelope detector fails to work.

This motivated us to implement CSS downlink on backscatter devices to combat interference and extend the receiving range. However, as we have introduced in Sec 2.2, the power-limited backscatter device is unable to afford the power consumption of carrier generation and signal down-conversion. Therefore, implementing chirp de-spreading seems to be infeasible on backscatter devices.

3.1 Passive Chirp De-spreading Design

With an understanding of the major cause of high power consumption in conventional chirp de-spreading, preliminarily,

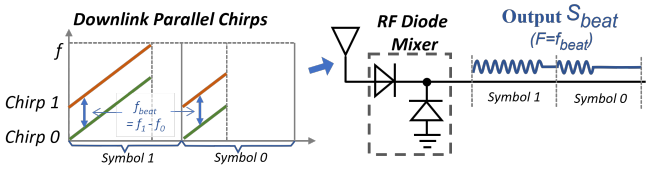

Figure 5: **Transmitted two chirps and circuit for passive chirp de-spreading**.

we explore uploading the task of carrier generation and down-chirp generation to the gateway. Specifically, we arrange the gateway to transmit two wide-band chirp signals into the air. By multiplying one chirp with another one, the receiver can achieve down-converting and de-spreading without the requirement of a locally generated carrier and the down-chirp signal.

The transmitted chirp signals are shown in Fig. 5, which are denoted by 'chirp_0' and 'chirp_1', respectively. They have the same chirp rate (i.e., frequency increasing rate whose unit is Hz/s), and hence there is a constant frequency difference between them. Unlike narrow-band signals, such as ASK signals or BFSK signals, these two wide-band chirp signals will not be covered by narrow-band interference.

These two chirps transmitted to the receiver can be written as:

$$chirp\_0(t) = cos\left[2\pi\left(f_0 t + 1/2ut^2\right)\right] \quad (1)$$

$$chirp\_1(t) = cos\left[2\pi\left(f_1 t + 1/2ut^2\right)\right] \quad (2)$$

where u is their chirp rate; f_0 and f_1 are their initial frequencies, respectively.

The receiver de-spreads these two chirps by multiplying them with each other using a passive, non-linear diode mixer. In practice, we use two diodes so as to receive the signal from the positive and negative terminals of the antenna. The result of signal mixing is expressed as:

$$\sum_{m=-\infty}^{+\infty}\sum_{n=-\infty}^{+\infty} a_{mn} cos\{2\pi([m(f_1+ut)+n(f_0+ut)]t\} \quad (3)$$

According to the property of non-linear mixing, we ignore the high-order harmonics as they have very low energy levels. Thus, we only consider the low-order harmonics, e.g., the first, second and third-order harmonics. More specifically, we can obtain a high-frequency signal and a low-frequency beat signal (denoted by S_{beat}) whose frequency is equal to the frequency difference $f_1 - f_0$. Instead of using FFT to detect the single tone, we use the LC resonator introduced in the next section to filter out the high-frequency signal.

Therefore, the only signal that can remain is the S_{beat}. If the receiver detects the presence of the S_{beat}, it can infer that the gateway is transmitting that two chirps. Moreover, by measuring the duration of the S_{beat}, the receiver can know the transmitting duration of the two chirps. This further allows

us to encode different symbols by varying this transmitting duration, as shown in Fig. 5.

3.2 Interference Resilience Analysis

From the measured spectrum shown in Fig. 4(b), it can be seen that the interference can be classified into two categories, i.e., narrow-band interference, and the spread spectrum signals. We consider signals using ASK, FSK and PSK modulation to be narrow-band signals, because they are composed of one or multiple narrow-band signal components with fixed frequencies.

Narrow-band interference: As we have introduced, narrow-band signals will be spread into the chirp's band in de-spreading process. More specifically, considering that there is a narrow-band interference with a fixed frequency f_n passes through the mixer with the two chirp signals, the resulting signals contain multiple components, including multiple high-order harmonics, the spread interference, and the envelope of all these signals. For example, if the interference signal is mixed with chirp_0 (Eq. 1), the generated signals are

$$\sum_{m=-\infty}^{+\infty}\sum_{n=-\infty}^{+\infty} a_{mn}cos\left\{2\pi\left[m(f_0+ut)+nf_n\right]t\right\}. \qquad (4)$$

where the high order harmonics and the spread interference with increasing frequency term (i.e., the ut in Eq. 4) cannot pass the following filter (i.e., the LC resonator). As for the envelope, it can hardly pass the filter unless it has the same frequency of $f_1 - f_0$. We argue that this case can hardly occur in practical scenarios.

Moreover, we should note that we also encountered strong out-of-band interference in our experiment (whose strength is about $12dB$ higher than that of chirp signals), and the passive mixer can only output the interference envelope instead of the desired beat frequency. This can be fixed with a SAW (Surface Acoustic Wave) filter.

Spread spectrum interference: Theoretically, our design can be interfered with by a specific type of chirp spread spectrum interference. This chirp signal should have the same chirp rate as the chirp signals transmitted by the gateway. Besides, the frequency difference between this interference chirp and one of the chirp signals transmitted by the gateway should be equal to $(f_1 - f_0)/2^n$ $(where\ n = 0,1,2,3...)$. According to our experiment, facing this type of interference, its anti-interference performance is similar to that of an envelope detector without an anti-interference design.

4 LNA-free Signal Magnification

Amplifying the received signals can enhance the receiving sensitivity and improve the receiving range. Receivers typically employ the LNA to achieve this. As we have introduced in Sec. 2.1, even the latest LNAs we can find, still consume several mA to hundreds of mA of external current. Hence, we are motivated to propose a signal magnification method with ultra-low power to replace the amplifier.

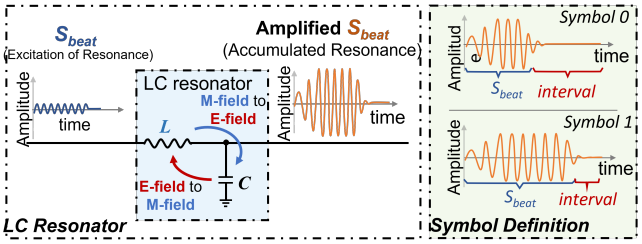

Figure 6: **Block Diagram of LNA-free Magnification.**

To achieve this, we explore accumulating the energy of the signal to implement magnification instead of consuming external current. We leverage an LC resonator to realize a container to accumulate energy. Conventionally, the LC resonator is used as high-frequency RF elements, e.g., on RF receiving antennas. It relies on tuning antenna impedance [3] to improve signal receiving efficiency at a particular frequency [1, 50]. Differing from these conventional uses, $\mu Mote$'s LC resonator works at relatively low frequencies (tens of kHz) and is used to accumulate the signal energy to magnify signal amplitude. Besides, when the signal energy is being accumulated, the signal's physical characteristics (e.g., frequency, amplitude, and phase which are used to carry data) will be destroyed. Thus, we should address the issue of information preservation during energy accumulation.

4.1 Magnifying by Accumulating Energy

In $\mu Mote$, the LC resonator is placed after the passive-CSS and consists of an inductor in series and a shunt capacitor, as shown in Fig. 6. The energy in this circuit will be alternatively transformed in the manner of magnetic and electric fields between the capacitor and inductors. The principle behind is the energy entered the magnetic field of the inductor can be used to charge the electric field on the capacitor plates, and vice versa. Similar to a pendulum or a swing, this "energy reciprocating" has its natural resonance frequency, which can be written as:

$$f_{res} = \frac{1}{2\pi\sqrt{L \cdot C_{res}}}$$

where C_{res} is the capacitance value of the capacitor in the resonant circuit.

The input signal of LC circuit is S_{beat}, the demodulated beat signal output by the passive-CSS circuit. If S_{beat} has the same frequency as $f_{resonant}$, its energy will be accumulated in the form of resonance for magnification, as shown in Fig. 6. Thus, the resonator acts as a magnifier and band-pass filter which only magnifies the voltage of S_{beat} whose frequency is f_{res}.

Table 1: Candidate *LC* resonators for different symbol rates

Symbol Rate	L	C_{res}	R_{inner}	Q	T_{dis}	V_{out}/V_{in}
$1\sim2kbps$	$0.05H$	$270pF$	273Ω	49	$600\mu s$	$40\times$
	$0.05H$	$270pF$	384Ω	35	$250\mu s$	$23\times$
	$0.05H$	**$270pF$**	**734Ω**	**18**	**$100\mu s$**	**$15\times$**
$5kbps$	$0.05H$	$470pF$	$1.1k\Omega$	9	$70\mu s$	$10\times$
	$0.05H$	**$470pF$**	**$1.3k\Omega$**	**7.9**	**$30\mu s$**	**$7\times$**

4.2 Preserve the Information

Unfortunately, this magnification scheme based on *LC* circuit can destroy the physical characteristics of the signal, e.g., the phase, the frequency and the amplitude of the signal. For instance, symbols in PSK (Phase-Shift-Keying) or ASK (Amplitude-Shift-Keying) manner can be destroyed as the phase and amplitude are instantaneous physical characteristics that cannot be preserved in an energy container. Therefore, we need to retain the encoding information in the energy accumulating.

Inspired by PIE (Pulse Interval Encoding), we leverage the duration of the magnified S_{beat} signal (i.e., S_{beat}'s energy) to represent the binary value of a symbol. The symbols representing binary bit "1" and binary bit "0" are shown in the right portion of Fig. 6. For simplicity, we refer to them as symbol "1" and symbol "0" respectively. Besides, in each symbol, there is an interval between two consecutive symbols. As the duration of S_{beat} in symbol "1" is longer than that in symbol "0", the symbol "1" contains more energy than symbol "0". The energy difference can further be distinguished by energy integration schemes introduced in Sec. 5.

To separate symbols, each symbol's energy should be released from *LC* circuit to avoid affecting the next symbol. In our scheme, we can separate symbols by assigning an interval between two symbols, as shown in the right portion of Fig. 6. In detail, during the symbol, the *LC* circuit has energy input and keeps resonating. During the interval, the energy of the current symbol stored in the *LC* resonator should be discharged by the circuit's internal resistance, or controlled discharging, see Sec.8.

4.3 Symbol Rate vs. Magnification Performance

From the symbol definition, we can see that a higher symbol rate requires a shorter interval, and fast discharging of *LC*. If the *LC* is not discharged completely, the residual energy will make the next symbol misidentified. Thus, we need a small Q factor to ensure sufficient discharging. On the other hand, a small Q means the weak magnification capability of the *LC* circuit. There is a trade-off between the magnification times and the symbol rate.

The Q factor is defined as

$$Q = 2\pi \frac{E_{store}}{P_{diss} T}$$

, where P_{diss} is the average dissipation power during a resonant period T, and E_{store} is the energy currently stored in *LC*. Hence, a higher Q factor means more energy can be preserved in *LC*, or more time to release the stored energy, i.e., discharge the capacitor in *LC*. On the other hand, the Q factor of the *LC* resonator can be calculated as:

$$Q = \frac{1}{R_{inner}} \cdot \sqrt{\frac{L}{C_{res}}}$$

where R_{inner} is the inner resistance of the *LC* resonator. From the two formulas, it can be seen that we can hardly calculate or measure the time constant of an *LC* resonator [48] to determine the required time interval for discharging. Further, it is also difficult to find COTS "*L*" and "*C*" components with the exact optimal value in practice. Hence, we empirically study *LC* resonators of different Q factors with available COTS components, and practically measure their discharging time.

We present the parameters of candidate *LC* resonators for different symbol rates in Table 1. In the table, "V_{out}/V_{in}" means the magnification ratio that the resonator can magnify the voltage of input S_{beat}, and the "T_{dis}" is the measured discharging time. For example, for a symbol rate of $2kbps$, we can choose parameters of the third resonator, whose discharging time is more than $100\mu s$. It means that the time interval of symbols should be more than $100\mu s$ also.

5 Low-power Decoding

With LNA-free magnification, we can get the magnified signals as well as symbols. The next step is to extract binary bits from the symbols. Mostly, ADC (Analog-to-Digital Conversion) is used for symbol decoding, but ADC will introduce high power consumption due to two reasons.

First, to ensure decoding accuracy, the ADC has to perform sampling tens of times when decoding each symbol. Based on Nyquist's theorem, the sampling rate should be twice the frequency of S_{beat}. Second, every single sampling operation of ADC consists of several complicated steps, e.g., extracting analog samples from a continuous signal, amplifying those analog samples to improve converting accuracy, integrating the amplified samples, and converting integration results to digital values. All aforementioned steps are controlled by an MCU or custom IC. As a result, even a well-known energy-efficient ADC [49] will consume more than a couple of 100 μW, which is two to three times higher than the total power consumption of our *µMote* including signal amplifying and symbol decoding.

In *µMote*, we carefully make use of the signal duration of S_{beat} and interval to represent symbols, as shown in Fig. 6. For

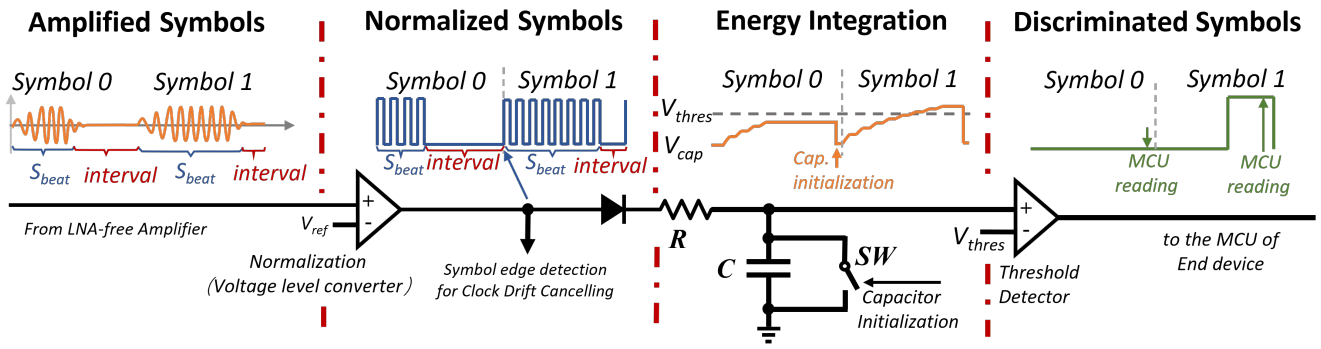

Figure 7: **Procedures for energy integration-based decoding.**

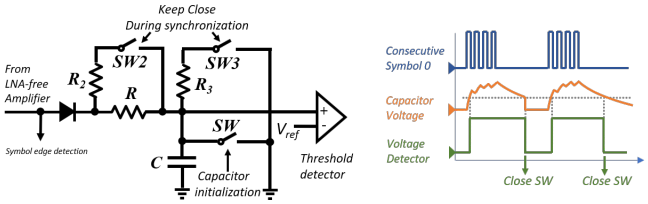

Figure 8: **The practical decoding circuit for symbol synchronization.**

example, symbol "1" has a shorter interval and longer signal duration than symbol "0", thus the energy of symbol "1" is higher than symbol "0". Different symbols to an *energy integrator* can result in different energy levels which can be used to discriminate symbols. Thus, a simple energy integrator can be employed to replace the ADC for decoding each symbol with only a single integration operation and low power consumption. *RC* (Resistance Capacitance) circuit is a typical realization of energy integrator as illustrated in Fig. 7. In order to save power, we can suppress the internal current to several μA with high resistance, and reduce the power consumption of integration to about $10\mu W$. As shown in Fig. 7, the signal S_{beat} can charge the capacitor "C" through the resistor "R" upon decoding. Because of the longer signal duration, symbol "1" can charge the capacitor to a higher peak voltage, which can be detected and converted to "1" by a threshold detector, and vice versa.

Apart from the basic design, there are several practical problems that need to be addressed.

Dynamic signal strength. In practice, the charged peak voltage in capacitor "C" is not only determined by S_{beat}'s duration, but also affected by S_{beat}'s strength. For example, if the receiver is placed close to the gateway, the incident signal power is high and hence the time to charge the capacitor would be short. In this case, a symbol "0" might be identified as a symbol "1". Conversely, if the receiver is placed far away, a symbol "1" may also be incorrectly identified as a symbol "0". To address this problem, we normalize S_{beat}'s amplitude after magnification. Specifically, we place a voltage level converter after the *LC* circuit and before the *RC* integrator, normalizing the amplitude of S_{beat} to a predefined reference voltage, as illustrated in the left part of Fig. 7. The detailed implementation of this circuit is introduced in Sec. 6 and its power consumption is discussed in Sec. 7.4.

Capacitor discharging. The binary value of each symbol is determined by how much S_{beat} charges the capacitor C. So the capacitor should be discharged fast and completely before the arrival of the next symbol to avoid inter-symbol interference. Intuitively, we can leverage the self-discharging of the capacitor. However, this is quite slow and thereby significantly slowing down the symbol rate. To address this problem, we add an NMOS switch to connect the positive plate of the capacitor to Ground (GND). At the end of each symbol, we make the capacitor directly connected to the Ground for fast discharging.

Symbol synchronization. To decode the symbol, the MCU should know exactly the end time of a symbol and read the output of the threshold detector at the time. Otherwise, the MCU may get the wrong integration results and misidentify symbols. In other words, it should be synchronized with the symbols sent by the gateway. Intuitively, we can make the gateway transmit preamble symbols for synchronization. However, if it is not synchronized, the decoding circuit and MCU cannot decode any symbols.

To achieve synchronization, the decoding circuit is programmed to switch to another structure which can detect preamble symbols. Specifically, two resistors and two NMOS switches are added to the circuit, as shown in the left portion of Fig. 8. Upon receiving the preamble, $SW2$ and $SW3$ are closed by the MCU so that resistors R_2 and R_3 are connected to the circuit. At this time, R and R_2 form a smaller resistor, accelerating the charging speed of the capacitor. With these resistors, a symbol "0" can rapidly charge the capacitor to the threshold of the detector, and the charged voltage can be released via R_3 and $SW3$ before the next symbol "0" arrives, as illustrated in Fig. 8. Thus, we can use a series of symbol "0" as the preamble, and the detector will output corresponding high voltage levels (the green line shown in Fig. 8) to inform the MCU that the preamble has arrived. The reason we do not use symbol "1" is that the duration of its S_{beat} signal is

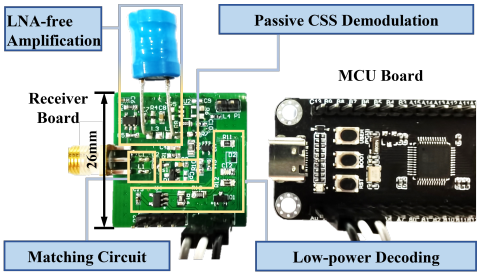

Figure 9: ***µMote* prototype.**

too long, so even with the presence of R_3, the voltage in the capacitor cannot be fully released before the next symbol "1" arrives.

Clock drift canceling. The clock on the backscatter device drifts over time, leading to synchronization and decoding errors. To address this, we present a method to cancel the clock drift. At the end of a symbol, we detect the first rising edge of the following symbol, as shown in Fig. 7. This rising edge represents the exact starting time of a symbol, which can be used to calibrate the clock on the device.

Power consumption. The decoding process requires three operations at the end of a symbol, i.e., reading the threshold detector, discharging the capacitor, and canceling the clock drift. These operations can be accomplished with less than 100 instructions, which incurs $< 1\%$ duty cycle and several μW power consuming. The necessary timing circuit to wake up the MCU and control the duty cycle is included in the MCU hardware, and the MCU only consumes nW-level power in low power mode [49].

Power optimization of *RC* circuit. We reduce the charging current to save power. The charging current can be written as

$$I_{charge} = \frac{V_{ref} \cdot exp(-t/RC)}{R}$$

, where V_{ref} is the charging voltage on the capacitor and is equal to the reference voltage in S_{beat} normalization. To suppress I_{charge}, we increase R and reduce C, and keep the product RC unchanged. For a symbol rate of $5kbps$, the proper values of R and C are $220k\Omega$ and $330pF$, and the power consumption of the RC circuit is $12\mu W$. The concrete evaluation results can be found in Sec. 7.

6 Implementation

We prototype $\mu Mote$ with COTS components on a $2.4cm \times 2.6cm$ PCB, as shown in Fig. 9. We introduce the hardware implementation as follows.

Matching circuit and passive-CSS demodulation: The matching circuit is composed of a series capacitor and a shunt inductor, as RF signals can easily pass through the capacitor but cannot go through the inductor to the Ground (GND). The matching circuit achieves reflection loss lower than $-20dB$ in the $913-916MHz$ frequency band, which is wide enough

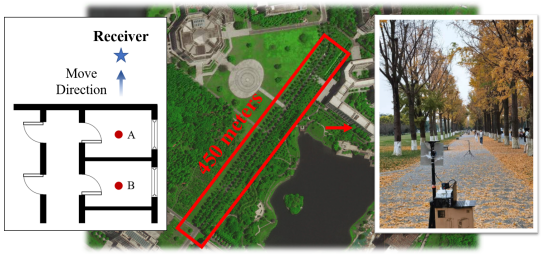

Figure 10: **Indoor and outdoor experiment environment.**

for receiving the two chirps. We use Skyworks SMS7630-005LF RF diodes as the passive mixer for down-conversion and de-spreading.

LNA-free Magnification: We implement $\mu Mote$ prototypes of three symbol rates. For $1kbps$ and $2kbps$, we choose the third resonator shown in Table 1. For $5kbps$, we choose the fifth one. The corresponding resonant frequencies of these two are $43kHz$ and $32.8kHz$. Before the LC resonator, we place a capacitor in series for DC-AC conversion, as the LC resonator requires AC input.

Normalization circuit: We employ a voltage level conversion circuit to normalize the magnified S_{beat}. In practical realization, we have two choices: (i) NCS2200, a comparator which has a relatively low power consumption of $18\mu W$ and can work on passive backscatter devices [64].(ii) MAX9914, which is actually a power-efficient operational amplifier which can also work as a voltage level converter. It can provide an extra sensitivity gain of $8dB$ with a power consumption of $51.17\mu W$, therefore further extending the receiving range. We use MAX9914 to realize the $\mu Mote$ prototype to explore the maximum range of our design. Besides, we use NCS2200 to realize a low power version of $\mu Mote$, which is named as "$\mu Mote-$" (i.e., "*µMote minus*"). Compared with $\mu Mote$, $\mu Mote-$ loses $8dB$ sensitivity but gains $33.17\mu W$ power saving.

RC Decoding circuit: We employ different combinations of R and C to build RC circuits for different symbol rates. The detailed values are introduced in Sec. 7.4. After the RC circuit, we use an S-1000C16 and an NLSV1T244 to build the threshold detector with a total power consumption of $1\mu W$. And we use GPIO ports of STM32L476 MCU to record the decoded data and control the circuit via three DMG2302UK NMOS switches. The MCU runs at a 1% duty cycle as we introduced in Sec. 5.

7 Evaluation

In this section, we first introduce the experiment setup in Sec. 7.1. Then we introduce benchmarks for subsequent evaluation in Sec. 7.2. Further, we evaluate communication ranges of $\mu Mote$ and benchmarks in Sec. 7.3. The power consumption comparison among our design and benchmarks, as well as $\mu Mote$ power breakdown, are illustrated in Sec. 7.4. Then we introduce interference experiments using interference signals

recorded in practice environments in Sec. 7.5.

7.1 Experiment Setup

We leverage a USRP-2922 to build the gateway's transmitter with an ADL5605-EVALZ [9] RF amplifier. Thus, the gateway can transmit up to $30dBm$ power, near the ImpinJ R420 RFID reader. The two downlink chirp signals are in $915MHz$ ISM band and their bandwidths are $1MHz$. The frequency difference (i.e., the frequency of S_{beat}) between the two chirp signals is set to the resonant frequencies of LC circuit, i.e., $43.3kHz$ for $1kbps$ and $2kbps$ symbol rates, and $32.8kHz$ for $5kbps$.

7.2 Benchmarks

- WISP5 [45]: a very widely known backscatter tag with an envelope detector-based receiver and an ADC for sampling. It has no amplification and anti-interference design. To favor the communication range test for the WISP5, we connect it with a $1.8V$ power supply module, instead of using its RF energy harvester which has an energy harvesting range of only several meters.

- Saiyan [17]: the very recent work that achieves LoRa symbol receiving with an envelope detector. Saiyan converts chirp symbols to amplitude-modulated signals via a SAW (Surface Acoustic Wave) filter, and uses an LNA for amplification. Following the literature [17] and the BOM (Bill of Material) list of their project document [16], we implement Saiyan hardware with a TQP3M9008 LNA and an OPA810 operational amplifier for signal amplification.

- Passive-DSSS [31]: an envelope detector-based design which employs two envelope detection channels for DSSS spreading codes to address interference. Besides, passive-DSSS employs a TLV9001 operational amplifier of $180\mu W$ to improve sensitivity and range.

Those benchmarks use their original encoding mechanisms, respectively, i.e., PIE for WISP5, chirp symbols for Saiyan, and DSSS spreading codes for passive-DSSS. For comparison, we manually set the symbol rate of those benchmarks to $1kbps$.

7.3 Communication Range

In this section, we first evaluate the receiving sensitivity of $\mu Mote$ and benchmarks using laboratory tests. Then we conduct outdoor experiments to evaluate their practical communication ranges in LOS (Line-of-Sight) scenario, i.e., a roughly straight road on campus, as shown in Fig. 10. Finally, we evaluate the communication range and packet throughput of

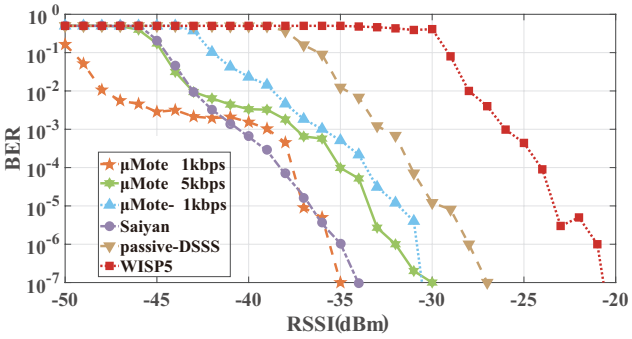

Figure 11: **Receiving sensitivity of $\mu Mote$ and benchmarks.**

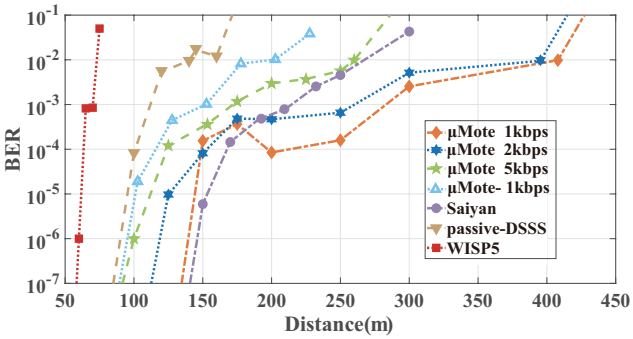

Figure 12: **Communication range in the outdoor LOS scenario.**

$\mu Mote$ in the NLOS (Non-Line-of-Sight) scenario. The NLOS experiment field is illustrated in the left portion of Fig. 10.

Receiving Sensitivity: Without interference, the receiving sensitivity theoretically determines the receiving range. In experiments, we measure the receiving sensitivity as the lowest received signal strength with a corresponding physical layer Bit Error Rate (BER) lower than 1%. To precisely control the signal strength, we connect the transmitter (i.e., USRP) and receiver with an RF cable and employ one or two $30dB$ RF attenuators in the cable. Thus, the receiving signal strength can be precisely controlled by setting the transmitting signal strength and the number of employed attenuators. Besides, to ensure accuracy, we leverage a professional signal strength meter [28] to calibrate the transmitting power of USRP. For each round, we measure the BER by sending $1,280,000$ bits.

The measured receiving sensitivities are shown in Fig. 11. It can be seen that the $\mu Mote$ has the best receiving sensitivity of $-48dBm$ at $1kbps$ symbol rate. According to theoretical estimation [10], its receiving range can reach 500 meters with the maximum transmitting power of our transmitter ($30dBm$). The receiving sensitivities of WISP5, replicated Saiyan, and passive-DSSS are $-28dBm$, $-43dBm$, and $-35dBm$. Similarly, we estimate their theoretical receiving ranges are $80m$, $250m$, and about $160m$, respectively. The sensitivity of $5kbps$ $\mu Mote$ prototype is $-43dBm$, due to the relatively low Q factor of LC circuit. The future solution to this is discussed in Sec. 8. Besides, $\mu Mote-$ has a sensitivity of about $-38dBm$, which is similar to Saiyan and better than passive-DSSS.

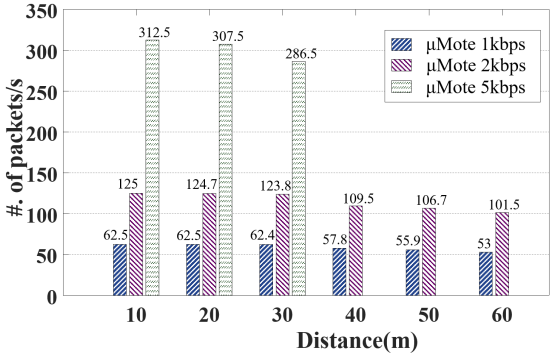

Figure 13: **Throughput of *µMote* for different bit rates when twin-CSS signal penetrates one wall.**

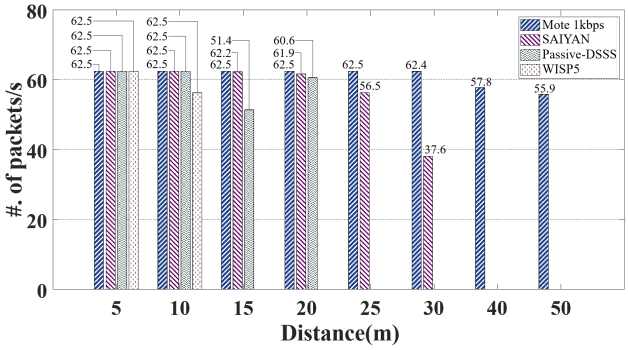

Figure 14: **Throughput of *µMote* 1*kbps* and benchmarks when the signal penetrates one wall.**

LOS Experiments: To evaluate the practical communication ranges of *µMote* and three benchmarks, we conduct outdoor experiments in LOS scenarios. The USRP transmits 30*dBm* RF signals through a 6*dBi* gain antenna, while each of the receivers uses a receiving antenna with 3*dBi* gain. We test *µMote* at different symbol rates of 1*kbps*, 2*kbps*, and 5*kbps*. Each BER value is obtained by counting misidentified bits in $1,280,000$ received bits.

The practical receiving ranges are shown in Fig. 12. At symbol rates of 1*kbps* and 2*kbps*, *µMote* achieves a similar receiving range of 400 meters, because at these symbol rates, the *LC* circuit has the same high *Q* factor and similar magnification performances. We do not reach the estimated 500*m* range, because we encountered strong in-band interference that came from unknown wireless devices and exceeded the anti-interference capability of our prototype. The practical ranges of WISP5, Saiyan and passive-DSSS are 70*m*, 250*m*, and 140*m*, which are similar to our estimations. We think that the reason is at these ranges, they do not face interference signals significantly stronger than signals transmitted by USRP. And the range of *µMote* 5*kbps* is 260*m* which is an expected result considering its sensitivity. Besides, *µMote*− achieves a maximum range of about 200*m*.

NLOS Experiments: We also measure the practical receiving ranges of *µMote* and benchmarks in the indoor NLOS scenarios, as a number of IoT devices are deployed in doors

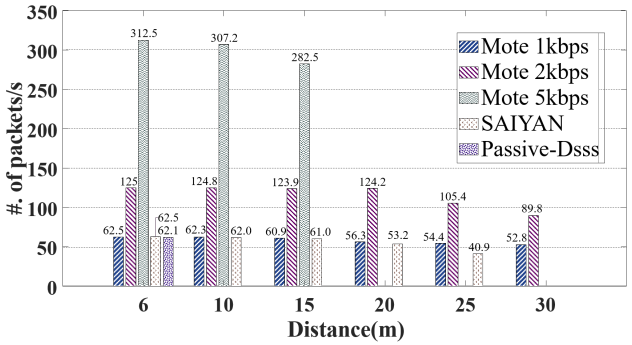

Figure 15: **Packet throughput of *µMote* and benchmarks when the signal penetrates two walls.**

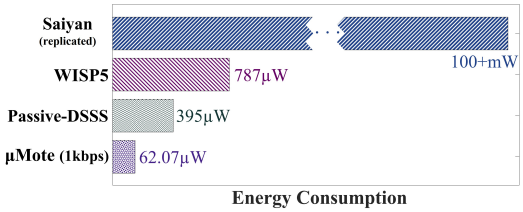

Figure 16: **The power consumption of *µMote* prototype and benchmarks.**

and signals have been attenuated by walls. The dots *A* and *B* represent where the gateway's USRP transmitter is located, and the star indicates where the receiver is placed. When the gateway is placed at the *A*, the transmitted signals have to penetrate one wall. When the gateway is at the dot *B*, the signals penetrate two walls. The star can be moved far or close to the transmitter to make different downlink ranges. We test three symbol rates with *µMote* and one symbol rate with benchmarks, and record each of the error bits in $1,280,000$ received bits.

Leveraging the recorded error bits, we calculate the packet throughput at different ranges, which can better represent the communication performance in actual environments. For example, even if there is only one error bit, the packet will become unrecognizable and is therefore discarded. The packet is defined as a 16-bit string, and thus the *packet throughput* refers to the number of received packets being correctly recognized. The test data is a packet which is sent for $10,000$ times in a loop.

When there is one wall, the measured packet throughput of *µMote* at different symbol rates are shown in Fig. 13. With 60*m* downlink range, the *µMote* receiver achieves 53 packets/*s* at 1*kbps*, and 101.5 packets/*s* at 2*kbps*. The maximum range for 5*kbps* is 30*m* and the corresponding throughput is 286.5 packets/*s*. We can learn from this result that for *µMote*, a *LC* resonator with high *Q* factor is crucial to achieving long range.

We also measure the packet throughput of benchmarks when their downlink signals penetrate one wall, and then compare them with *µMote* at 1*kbps*. The results are plotted

Table 2: Power breakdown of two prototypes

Modules	Despreading	Magnification	Regulator	*RC* Decoding (1*kbps*)	MCU (1% duty cycle)	Total
μMote	0μW	0μW	51.17μW	3.4μW	7.5μW	62.07μW
μMote−	0μW	0μW	18μW	3.4μW	7.5μW	28.9μW

Table 3: Parameters of *RC* decoding circuit for different symbol rates

Bit rate	***R* value**	***C* value**	***E*/symbol**	**Power**
1kbps	910$k\Omega$	330pF	2.40nJ/bit	3.4μW
2kbps	470$k\Omega$	330pF	2.36nJ/bit	3.72μW
5kbps	200$k\Omega$	330pF	2.51nJ/bit	13.55μW

in Fig. 14. Among these benchmarks, Saiyan has the longest range of 30m with a packet throughput of 37.6 packets/s, this range is half the range of *μMote* (i.e., 60m at 1$kbps$).

When there are two walls between the gateway and receivers, the receiving ranges are further decreased, as shown in Fig. 15. At the range of 30m, *μMote* has acceptable throughput values of 52.8 packets/s at 1$kbps$ and 89.8 packets/s at 5$kbps$. Saiyan and passive-DSSS can receive at the ranges of 25m and 6m, with packet throughput values of 61.6 packets/s and 62.1 packets/s, respectively. WISP5 cannot receive its downlink signal.

7.4 Power Consumption

μMote vs. Benchmarks: To demonstrate the power-efficiency of our design, we measure the practical power consumption of *μMote* prototypes and benchmarks using a sub-μA-level power monitor [52]. The results are plotted in Fig. 16. We can see that the total power consumption of *μMote* (1$kbps$) is 61.07μW, which is the lowest. WISP5 and passive-DSSS have a power consumption of several hundreds of μW, as we take the power consumption of ADC sampling and the MCU for ADC control into account. We replicated Saiyan prototype according to the BOM extracted from their project files [16, 17]. At its maximum receiving range, the power consumption of the Saiyan prototype is 446mW. We believe the cause of this high power consumption is their use of two amplifiers [21, 40].

μMote power breakdown: Table 2 shows the power breakdown of the *μMote* prototype. The de-spreading circuit and magnification circuit consume zero power as they are driven by the received signal. For different symbol rates, the corresponding power consumption of *RC* decoding circuit (including the threshold detector) is illustrated in Table 3. It can be observed that at different symbol rates, the energy budget for decoding one bit remains roughly unchanged. The cause is that the energy budget is related to capacitance. The MCU average power consumption is about 7.5μW with 1% duty cycle.

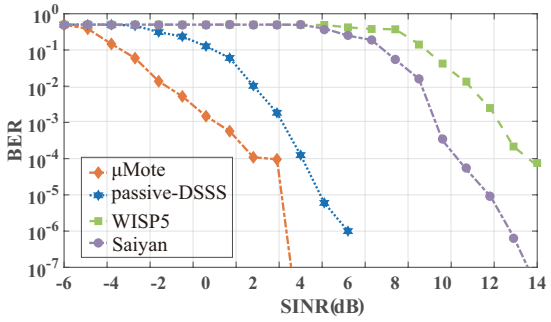

Figure 17: **Receiving BER of *μMote* and benchmarks under LoRa interference.**

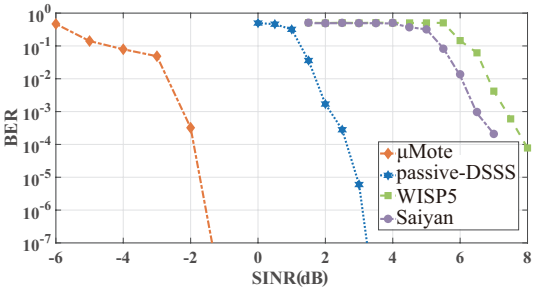

Figure 18: **Receiving BER of *μMote* and benchmarks under RFID interference.**

7.5 Interference Resilience

We evaluate the interference resilience of *μMote* under interference in 900MHz ISM band, such as RFID and LoRa. We use the interference-resilient receiver, i.e., passive-DSSS, as benchmarks. We also evaluate WISP5 and Saiyan for comparison, which are not interference-resilient. We choose the impinj R420 RFID reader and EBYTE E32-915T30S Lora transceiver as the interference source. Then we use USRP to record practical signals transmitted by these two devices, so we can manually amplify or attenuate the recorded signals to make interference with different strengths. Finally, we leverage RF cables to transmit twin-CSS signals as well as those interference signals to *μMote* receiver to measure receiving BER values. Both *μMote* receiver and passive-DSSS receiver are set to 1$kbps$ symbol rate. The bandwidths of RFID and LoRa interference are set to 100kHz and 500kHz, respectively.

Fig. 17 and Fig. 18 show the BER measurement under LoRa and RFID interference signals. The results demonstrate that the *μMote* prototype can operate under negative SINR caused by RFID or LoRa interference. In detail, at BER of

1%, the corresponding SINRs caused by LoRa or RFID signal are about $-1dB$ and $-2.7dB$, whereas at BER of 0.1% the SINRs caused by LoRa or RFID signal are about $-1dB$ and $-2.2dB$. We can learn *µMote* can operate under negative SINR caused by LoRa and RFID interference. Passive-DSSS has SINR improvement over classic WISP5 which has no anti-interference design, but it cannot work under negative SINR.

8 Discussion and Limitations

Accessing multiple devices or gateways: To date, *µMote* cannot support concurrent transmissions from the gateway to multiple backscatter devices, as *µMote* has no frequency division or other multiple access designs. A feasible solution is to employ time division on the MAC layer, similar to RFID protocols. In addition, *µMote* fails to work in the face of the hidden node problem, which occurs when multiple gateways want to talk with a certain receiver, but they are unaware of each other's existence.

Strength loss: The gateway transmitter needs to split its power across both chirps, and therefore it may require more transmitting power than it would have been needed to transmit to a device at the same distance using a conventional active receiver. Although *µMote* mixes the two chirps, the generated harmonics will also result in a loss of signal energy.

Spectrum efficiency: The bandwidth consumed in our design is about $1.04MHz$ ($1MHz$ chirp and $43kHz$ S_{beat}). Most spectrum bandwidth is spent on spectrum spread to resist interference. Compared with LoRa receivers, our *µMote* consumes similar spectrum bandwidth but achieves power consumption three orders of magnitude lower than LoRa.

Improving symbol rate: As the trade-off introduced in Sec. 4, in this paper, we cannot achieve the highest symbol rate and best magnification performance simultaneously. Improving the magnification performance requires increasing the interval time for discharging the *LC* resonator, while improving the symbol rate requires decreasing the interval time. Hence, we explore a discharging mechanism to the *LC* resonator. Specifically, when the symbol synchronization is completed, we can discharge the *LC* resonator at the middle (to discharge the energy of symbol "0") and the end of a symbol. Thus, the energy in *LC* can be discharged more rapidly to allow a higher symbol rate, even for *LC* of very high *Q* factor to gain high magnification performance. Moreover, we also plan to explore whether we can add more threshold detector modules ($< 1\mu W$ per module) with different thresholds, and then the symbols can be quantified into more characters, thereby increasing the bit rate.

9 Related Work

Diode-based mixer. Similar to *µMote*, there are two existing works [11, 42, 43] that use the diode mixer [4] to mix two RF signals and achieve low-power subcarrier generation or very high-speed receiving. The differences between our work and them are three-fold. The first difference is waveform modulation. In *µMote* design, we employ Chirp Spread Spectrum (CSS) signals as downlink signals, and thus our work can combat interference and even work under negative SINR. The second difference lies in *µMote*'s system design. The passive chirp de-spreading scheme should be used in conjunction with the *LC* resonator which acts as a magnifier and filter, otherwise the signal strength loss due to chirp mixing would decrease the receiving range, and the receiver cannot filter or detect the generated beat signal. The third difference is our design has the benefit of a relatively long receiving distance.

Long-range backscatter communication. To resist interference and improve communication range in low-power IoT systems, tremendous backscatter innovations [23, 35, 37, 51, 54, 55] leverage CSS modulation on LoRa, extending the uplink range to more than one kilometer. Nevertheless, these designs cannot receive spread spectrum signals on the downlink, as spread spectrum signal demodulation and de-spreading involve high-power local carrier generation and computing-intensive correlation for synchronizing local de-spreading codes or de-spreading signals. This fact causes unbalanced communication ranges and robustness on uplink and downlink. Moreover, tunnel diode can be employed in backscatter transmitters, further increasing the communication range of backscatter devices [56].

Saiyan [17] employs a SAW filter to re-shape the envelope of chirp signals, enabling an envelope detector to receive LoRa signals on the downlink. But this method does not de-spread chirps so it cannot gain the communication range and robustness improvements of CSS, and instead, it has to use LNA to boost range. Passive-DSSS [31] receives both spreading codes and synchronized de-spreading codes from the transmitter, first achieving the DSSS communication on envelope detector-based receivers. Compared with *µMote* which employs a passive mixer to de-spread two parallel chirps, Passive-DSSS relies on envelope detectors to receiver signal, and hence it cannot receive CSS signals and work under negative SINR. Moreover, Passive-DSSS does not contain any low-power signal magnifying scheme (e.g., the LC resonator) and low-power ADC-free decoding scheme, resulting in a relatively limited receiving range and relatively high decoding power.

Signal magnification techniques. The most commonly used signal amplification means is the LNA. As we introduce in Sec. 2.1, even the latest commercial LNA ICs consume more than several *mW* of power. To magnify signals with low power, recent researches leverage the principle of *Voltage transforming* or *Impedance tuning* to get signals with mag-

nified voltages. For example, XSHIFT [43] leverage a coil voltage transformer to magnify the voltage of demodulated signals by 5 times. Besides, *LC* circuits are also used to boost the voltage of received RF signal by adjusting the antenna impedance [1, 50]. However, these two methods cannot magnify the instantaneous power of RF signals or demodulated signals, so their improvements in receiving sensitivities are relatively limited, compared to our design.

Backscatter communication. Our work is also related to backscatter communication techniques, as *µMote* characteristics have potential benefits existing backscatter devices. For LoRa backscatter devices [23, 35, 37, 51, 54, 55], it can make up for their limited downlink performance in terms of range and robustness against interference, with only μW-level power. For other tremendous backscatter innovations features of high data rate [53], high-throughput [24, 25, 42], robustness [57], large system scale [19], simplified hardware [30, 43, 62], and ambient-signal-compatible [2, 5, 12, 22, 26, 27, 32, 33, 35, 36, 38, 54, 61, 63], *µMote* can provide downlink connection with benefits of interference-resistant, low-power, and cost-efficiency, at the same time.

ADC-free decoding. Similar to *µMote*, RFID tags [10] can decode PIE symbols without ADC. But differing from *µMote*, the PIE decoder of RFID tags can extract the synchronization clock from PIE symbols by simply inverting the PIE waveform (which is illustrated in the citation [28]). However, according to the symbol definition of our design, our ADC-free decoding circuit cannot extract the synchronization clock in the same way as RFID tags. Hence, we have to explore a dedicated synchronization scheme for our decoding circuit.

Wake-up receiver. Due to the power benefit of integrated circuits, envelope detector-based wake-up ICs achieve power consumption of less than $100\mu W$ and good receiving sensitivity of lower than $-60dBm$. These receivers typically has a low power consumption of less than $100\mu W$, and provide sensitivities lower to $-60dBm$ [20, 39, 44]. There are two distinctions between our work and these ICs. First, our design enables interference-resistant communication with μW-level power. Second, employing the LC resonator and the dedicated encoding mechanism can magnify the amplitude of demodulated signals, which is a potential alternative technique for receivers to enhance the receiving sensitivity.

10 Conclusion

In this paper, we systematically investigate the issue of low-power and long-range receiving, the critical bottleneck of communication of backscatter devices. We present *µMote*, an μW-power receiver with 400 meters range. We design and implement the first passive chirp de-spreading method with a simple mixer by offloading high-power carrier de-chirp generating to the gateway. Then we present a novel zero-power magnification method with a *LC* resonant circuit, effectively improving the receiving sensitivity. We propose an energy integration-based decoding mechanism instead of high-power ADC sampling to reduce power consumption. We conduct extensive experiments in different scenarios. The evaluation shows that *µMote* can support up to 400m receiving range with $62.07\mu W$ power consumption at $2kbps$ symbol rate. Compared to benchmarks, *µMote* improves the downlink range by $2.5\times$ to $8.65\times$, with a power consumption reduction of 63.2% to even three orders of magnitude.

Acknowledgments

We sincerely thank our shepherd and all reviewers for their time in reviewing our paper and providing valuable feedback. This paper is partially supported by the National Natural Science Foundation of China under Grant U21A20462; National Key R&D Program of China under Grant 2022YFC3801302; National Natural Science Foundation of China under Grant U22A2031; National Key R&D Program of China under Grant 2021QY0703; National Natural Science Foundation of China under Grants 61872061, 61932013 and 61872285.

References

[1] Mohamed R Abdelhamid, Ruicong Chen, Joonhyuk Cho, Anantha P Chandrakasan, and Fadel Adib. Self-reconfigurable micro-implants for cross-tissue wireless and batteryless connectivity. In *MobiCom'20: Proceedings of the 26th Annual International Conference on Mobile Computing and Networking*, 2020.

[2] Ali Abedi, Farzan Dehbashi, Mohammad Hossein Mazaheri, Omid Abari, and Tim Brecht. Witag: Seamless wifi backscatter communication. In *Proceedings of the Annual conference of the ACM Special Interest Group on Data Communication on the applications, technologies, architectures, and protocols for computer communication*, pages 240–252, 2020.

[3] All about circuits. Applications of resonance. https://www.allaboutcircuits.com/textbook/alternating-current/chpt-6/applications-of-resonance/, 2021.

[4] Mark R Barber. Noise figure and conversion loss of the schottky barrier mixer diode. *IEEE Transactions on Microwave Theory and Techniques*, 15(11):629–635, 1967.

[5] Dinesh Bharadia, Kiran Raj Joshi, Manikanta Kotaru, and Sachin Katti. Backfi: High throughput wifi backscatter. In *Proceedings of the 2015 ACM Conference on Special Interest Group on Data Communication*, SIGCOMM '15, pages 283–296, New York, NY, USA, 2015. ACM.

[6] Estarija Dan David, Katreena Gabrielle Juntado, Miguel Lorenzo Panagsagan, Anastacia Alvarez, Maria Theresa De Leon, Marc Rosales, John Richard Hizon, and Christopher Santos. Design and implementation of a baseband lora demodulator using de-chirp method. In *2019 International Symposium on Multimedia and Communication Technology (ISMAC)*, pages 1–4, 2019.

[7] Analog Devices. Adl9005. https://www.analog.com/media/en/technical-documentation/data-sheets/adl9005.pdf, 2021.

[8] Analog Devices. Hmc8412chips. https://www.analog.com/media/en/technical-documentation/data-sheets/hmc8412chips.pdf, 2021.

[9] Analog Devices. Evalz-adl5605. https://www.analog.com/en/design-center/evaluation-hardware-and-software/evaluation-boards-kits/eval-adl5605.html$#$eb-overview, 2022.

[10] Daniel Dobkin. *The rf in RFID: uhf RFID in practice*. Newnes, 2012.

[11] Joshua F Ensworth, Alexander T Hoang, and Matthew S Reynolds. A low power 2.4 ghz superheterodyne receiver architecture with external lo for wirelessly powered backscatter tags and sensors. In *2017 IEEE International Conference on RFID (RFID)*, pages 149–154. IEEE, 2017.

[12] Joshua F Ensworth and Matthew S Reynolds. Every smart phone is a backscatter reader: Modulated backscatter compatibility with bluetooth 4.0 low energy (ble) devices. In *2015 IEEE International Conference on RFID (RFID)*, pages 78–85, April 2015.

[13] EPCglobal. Epc radio-frequency identity protocols class-1 generation-2 uhf rfid protocol for communications at 860 mhz - 960 mhz version 1.2.0, 2008.

[14] Inc. Freescale Semiconductor. Practical considerations for low noise amplifier design - white paper. https://www.nxp.com/docs/en/white-paper/RFLNAWP.pdf, 2013.

[15] Jeremy Gummeson, Shane S Clark, Kevin Fu, and Deepak Ganesan. On the limits of effective hybrid micro-energy harvesting on mobile crfid sensors. In *Proceedings of the 8th international conference on Mobile systems, applications, and services*, pages 195–208. ACM, 2010.

[16] Xiuzhen Guo. Saiyan-the design and implementation of a low-power demodulator for lora backscatter systems. https://github.com/ZangJac/Saiyan, 2022.

[17] Xiuzhen Guo, Longfei Shangguan, Yuan He, Nan Jing, Jiacheng Zhang, Haotian Jiang, and Yunhao Liu. Saiyan: Design and implementation of a low-power demodulator for {LoRa} backscatter systems. In *19th USENIX Symposium on Networked Systems Design and Implementation (NSDI 22)*, pages 437–451, 2022.

[18] Xiuzhen Guo, Longfei Shangguan, Yuan He, Jia Zhang, Haotian Jiang, Awais Ahmad Siddiqi, and Yunhao Liu. Aloba: Rethinking on-off keying modulation for ambient lora backscatter. In *Proceedings of the 18th Conference on Embedded Networked Sensor Systems*, pages 192–204, 2020.

[19] Mehrdad Hessar, Ali Najafi, and Shyamnath Gollakota. Netscatter: Enabling large-scale backscatter networks. In *Proceedings of the 16th USENIX Conference on Networked Systems Design and Implementation*, NSDI'19, pages 271–283, USA, 2019. USENIX Association.

[20] Xiongchuan Huang, Pieter Harpe, Guido Dolmans, Harmke de Groot, and John R Long. A 780–950 mhz, 64–146 μw power-scalable synchronized-switching ook receiver for wireless event-driven applications. *IEEE Journal of Solid-State Circuits*, 49(5):1135–1147, 2014.

[21] Texas Instruments. Opa810. https://www.ti.com/product/OPA810/part-details/OPA810IDCKR, 2022.

[22] Vikram Iyer, Vamsi Talla, Bryce Kellogg, Shyamnath Gollakota, and Joshua Smith. Inter-technology backscatter: Towards internet connectivity for implanted devices. In *Proceedings of the 2016 ACM SIGCOMM Conference*, SIGCOMM'16, pages 356–369, New York, NY, USA, 2016. Association for Computing Machinery.

[23] Jinyan Jiang, Zhenqiang Xu, Fan Dang, and Jiliang Wang. Long-range ambient lora backscatter with parallel decoding. In *Proceedings of the 27th Annual International Conference on Mobile Computing and Networking*, pages 684–696, 2021.

[24] Meng Jin, Yuan He, Xin Meng, Dingyi Fang, and Xiaojiang Chen. Parallel backscatter in the wild: When burstiness and randomness play with you. In *Proceedings of the 24th Annual International Conference on Mobile Computing and Networking*, pages 471–485, 2018.

[25] Meng Jin, Yuan He, Xin Meng, Yilun Zheng, Dingyi Fang, and Xiaojiang Chen. Fliptracer: Practical parallel decoding for backscatter communication. *IEEE/ACM Transactions on Networking*, 27(1):330–343, 2019.

[26] Bryce Kellogg, Aaron Parks, Shyamnath Gollakota, Joshua R. Smith, and David Wetherall. Wi-fi backscatter: Internet connectivity for rf-powered devices. In *Proceedings of the 2014 ACM Conference on SIGCOMM*,

SIGCOMM '14, pages 607–618, New York, NY, USA, 2014. Association for Computing Machinery.

[27] Bryce Kellogg, Vamsi Talla, Shyamnath Gollakota, and Joshua R. Smith. Passive wi-fi: Bringing low power to wi-fi transmissions. In *Proceedings of the 13th Usenix Conference on Networked Systems Design and Implementation*, NSDI'16, pages 151–164, USA, 2016. USENIX Association.

[28] Keysight. E4418b epm series single-channel power meter. https://www.keysight.com/us/en/product/E4418B/epm-series-singlechannel-power-meter.html, 2021.

[29] A. Kokkeler, N. B. Molenkamp, and S. H. Gerez. A comparison of fft processor designs. 2013.

[30] Songfan Li, Chong Zhang, Yihang Song, Hui Zheng, Lu Liu, Li Lu, and Mo Li. Internet-of-microchips: direct radio-to-bus communication with spi backscatter. In *Proceedings of the 26th Annual International Conference on Mobile Computing and Networking*, pages 1–14, 2020.

[31] Songfan Li, Hui Zheng, Chong Zhang, Yihang Song, Shen Yang, Minghua Chen, Li Lu, and Mo Li. Passive {DSSS}: Empowering the downlink communication for backscatter systems. In *19th USENIX Symposium on Networked Systems Design and Implementation (NSDI 22)*, pages 913–928, 2022.

[32] Yan Li, Zicheng Chi, Xin Liu, and Ting Zhu. Passive-zigbee: Enabling zigbee communication in iot networks with 1000x+ less power consumption. In *Proceedings of the 16th ACM Conference on Embedded Networked Sensor Systems*, SenSys '18, pages 159–171, New York, NY, USA, 2018. Association for Computing Machinery.

[33] Vincent Liu, Aaron Parks, Vamsi Talla, Shyamnath Gollakota, David Wetherall, and Joshua R. Smith. Ambient backscatter: Wireless communication out of thin air. In *Proceedings of the ACM SIGCOMM 2013 Conference on SIGCOMM*, SIGCOMM '13, pages 39–50, New York, NY, USA, 2013. Association for Computing Machinery.

[34] microsemi. Zl30260-zl30263. https://www.microsemi.com/document-portal/doc_download/136349-zl30260-zl30263-datasheet, 2022.

[35] Rajalakshmi Nandakumar, Vikram Iyer, and Shyamnath Gollakota. 3d localization for sub-centimeter sized devices. In *Proceedings of the 16th ACM Conference on Embedded Networked Sensor Systems*, SenSys '18, pages 108–119, New York, NY, USA, 2018. Association for Computing Machinery.

[36] Aaron N. Parks, Angli Liu, Shyamnath Gollakota, and Joshua R. Smith. Turbocharging ambient backscatter communication. In *Proceedings of the 2014 ACM Conference on SIGCOMM*, SIGCOMM '14, pages 619–630, New York, NY, USA, 2014. Association for Computing Machinery.

[37] Yao Peng, Longfei Shangguan, Yue Hu, Yujie Qian, Xianshang Lin, Xiaojiang Chen, Dingyi Fang, and Kyle Jamieson. Plora: A passive long-range data network from ambient lora transmissions. In *Proceedings of the 2018 Conference of the ACM Special Interest Group on Data Communication*, SIGCOMM '18, pages 147–160, New York, NY, USA, 2018. Association for Computing Machinery.

[38] Carlos Pérez-Penichet, Frederik Hermans, Ambuj Varshney, and Thiemo Voigt. Augmenting iot networks with backscatter-enabled passive sensor tags. In *Proceedings of the 3rd Workshop on Hot Topics in Wireless*, pages 23–27. ACM, 2016.

[39] Nathan M Pletcher, Simone Gambini, and Jan M Rabaey. A 2ghz 52 μw wake-up receiver with-72dbm sensitivity using uncertain-if architecture. In *2008 IEEE International Solid-State Circuits Conference-Digest of Technical Papers*, pages 524–633. IEEE, 2008.

[40] Qorvo. Tqp3m9008 high linearity lna gain block. https://www.qorvo.com/products/p/TQP3M9008, 2022.

[41] Aanjhan Ranganathan, Boris Danev, and Srdjan Capkun. Low-power distance bounding. *arXiv preprint arXiv:1404.4435*, 2014.

[42] Mohammad Rostami, Xingda Chen, Yuda Feng, Karthikeyan Sundaresan, and Deepak Ganesan. Mixiq: re-thinking ultra-low power receiver design for next-generation on-body applications. In *Proceedings of the 27th Annual International Conference on Mobile Computing and Networking*, pages 364–377, 2021.

[43] Mohammad Rostami, Karthik Sundaresan, Eugene Chai, Sampath Rangarajan, and Deepak Ganesan. Redefining passive in backscattering with commodity devices. In *Proceedings of the 26th Annual International Conference on Mobile Computing and Networking*, pages 1–13, 2020.

[44] Camilo Salazar, Andreia Cathelin, Andreas Kaiser, and Jan Rabaey. A 2.4 ghz interferer-resilient wake-up receiver using a dual-if multi-stage n-path architecture. *IEEE Journal of Solid-State Circuits*, 51(9):2091–2105, 2016.

[45] Aaron Parks & samannp. Wisp 5 - hw. https://github.com/wisp/wisp5-hw, 2017.

[46] Alanson P Sample, Daniel J Yeager, Pauline S Powledge, Alexander V Mamishev, and Joshua R Smith. Design of an rfid-based battery-free programmable sensing platform. *IEEE Transactions on Instrumentation and Measurement*, 57(11):2608–2615, 2008.

[47] Bill Schweber. Understanding the basics of low-noise and power amplifiers in wireless designs. https://www.digikey.com/en/articles/understanding-the-basics-of-low-noise-and-power-amplifiers-in-wireless-designs, 2013.

[48] CADENCE PCB SOLUTIONS. What is the time constant of an rlc circuit? https://resources.pcb.cadence.com/blog/2020-what-is-the-time-constant-of-an-rlc-circuit, 2020.

[49] STMicroelectronics. Stm32l4 series. https://www.st.com/en/microcontrollers-microprocessors/stm32l4-series.html, 2021.

[50] Mark Stoopman, Shady Keyrouz, Hubregt J Visser, Kathleen Philips, and Wouter A Serdijn. Co-design of a cmos rectifier and small loop antenna for highly sensitive rf energy harvesters. *IEEE Journal of Solid-State Circuits*, 49(3):622–634, 2014.

[51] Vamsi Talla, Mehrdad Hessar, Bryce Kellogg, Ali Najafi, Joshua R. Smith, and Shyamnath Gollakota. Lora backscatter: Enabling the vision of ubiquitous connectivity. *Proc. ACM Interact. Mob. Wearable Ubiquitous Technol.*, 1(3), September 2017.

[52] Taobao. Eka950 0.1μa-level power monitor. https://https://m.tb.cn/h.U1A802y?tk=1u3A2wmBIRx, 2021.

[53] Stewart Thomas and Matthew S Reynolds. Qam backscatter for passive uhf rfid tags. In *2010 IEEE International Conference on RFID (IEEE RFID 2010)*, pages 210–214. IEEE, 2010.

[54] Ambuj Varshney, Oliver Harms, Carlos Pérez-Penichet, Christian Rohner, Frederik Hermans, and Thiemo Voigt. Lorea: A backscatter architecture that achieves a long communication range. In *Proceedings of the 15th ACM Conference on Embedded Network Sensor Systems*, pages 1–14, 2017.

[55] Ambuj Varshney, Carlos Pérez Penichet, Christian Rohner, and Thiemo Voigt. Towards wide-area backscatter networks. In *Proceedings of the 4th ACM Workshop on Hot Topics in Wireless*, pages 49–53, 2017.

[56] Ambuj Varshney, Wenqing Yan, and Prabal Dutta. Judo: addressing the energy asymmetry of wireless embedded systems through tunnel diode based wireless transmitters. In *Proceedings of the 20th Annual International Conference on Mobile Systems, Applications and Services*, pages 273–286, 2022.

[57] Jue Wang, Haitham Hassanieh, Dina Katabi, and Piotr Indyk. Efficient and reliable low-power backscatter networks. In *Proceedings of the ACM SIGCOMM 2012 Conference on Applications, Technologies, Architectures, and Protocols for Computer Communication*, SIGCOMM '12, pages 61–72, New York, NY, USA, 2012. Association for Computing Machinery.

[58] Wikipedia. Low noise amplifier. https://en.wikipedia.org/wiki/Low-noise_amplifier, 2022.

[59] Die Wu, Muhammad Jawad Hussain, Songfan Li, and Li Lu. R2: Over-the-air reprogramming on computational rfids. In *2016 IEEE International Conference on RFID (RFID)*, pages 1–8, 2016.

[60] Wenyu Yang, Die Wu, Muhammad Jawad Hussain, and Li Lu. Wireless firmware execution control in computational rfid systems. In *2015 IEEE International Conference on RFID (RFID)*, pages 129–136, 2015.

[61] Pengyu Zhang, Dinesh Bharadia, Kiran Joshi, and Sachin Katti. Hitchhike: Practical backscatter using 54 commodity wifi. In *Proceedings of the 14th ACM Conference on Embedded Network Sensor Systems CD-ROM*, SenSys '16, pages 259–271, New York, NY, USA, 2016. Association for Computing Machinery.

[62] Pengyu Zhang, Pan Hu, Vijay Pasikanti, and Deepak Ganesan. Ekhonet: High speed ultra low-power backscatter for next generation sensors. In *Proceedings of the 20th annual international conference on Mobile computing and networking*, pages 557–568. ACM, 2014.

[63] Renjie Zhao, Fengyuan Zhu, Yuda Feng, Siyuan Peng, Xiaohua Tian, Hui Yu, and Xinbing Wang. Ofdma-enabled wi-fi backscatter. In *The 25th Annual International Conference on Mobile Computing and Networking*, MobiCom '19, pages 20:1–20:15, New York, NY, USA, 2019. ACM.

[64] Yi Zhao, Joshua R Smith, and Alanson Sample. Nfc-wisp: A sensing and computationally enhanced near-field rfid platform. In *2015 IEEE International Conference on RFID (RFID)*, pages 174–181. IEEE, 2015.